JOURNAL OF SOLID STATE CHEMISTRY **133,** 347–355 (1997)
ARTICLE NO. SC977581

Characterization of Beryllium–Boron-Bearing Materials by Parallel Electron Energy-Loss Spectroscopy (PEELS)

Laurence A. J. Garvie,*,[1] Peter R. Buseck,* and Peter Rez†

* *Departments of Geology and Chemistry/Biochemistry, Arizona State University, Tempe, Arizona 85282;*
† *Center for Solid State Science and Department of Physics and Astronomy, Arizona State University, Tempe, Arizona 85287-1704*

Received August 4, 1997; accepted August 4, 1997

The stoichiometry of a set of commercial and laboratory-synthesized Be–B-bearing materials was determined by parallel electron energy-loss spectroscopy (PEELS). The Be and B K edges are well separated in energy, allowing easy determination of the elemental ratios. PEELS analyses of materials with reported compositions of "Be_2B" and "Be_2B_3" provided stoichiometries near $Be_{2.8}B$ and Be_4B_5, respectively. We confirmed an earlier report of $Be_{0.6(\pm0.1)}B_{5.9(\pm0.7)}C$, a material with the α-rhombohedral B structure. We also synthesized and characterized $Be_{0.5(\pm0.1)}B_{4.9(\pm0.3)}N$, a new ternary material with the α-rhombohedral B structure with refined hexagonal cell parameters of a_h=5.487(5) Å and c_h=12.486(14) Å. By comparison of the features at the core-loss edges of $Be_{0.5(\pm0.1)}B_{4.9(\pm0.3)}N$, we conclude that most N forms N_2 pairs between the icosahedra and Be substitutes for B within the icosahedra.

1. INTRODUCTION

Electron energy-loss spectroscopy (EELS) is well suited for Be and B analysis since their K core-loss edges are well separated in energy (Fig. 1), allowing easy determination of the elemental ratios. The spectra can be used for quantitative chemical analysis of small regions of sample, i.e., at high spatial resolutions. Interpretation of the energy-loss near-edge structures (ELNES) of the core-loss edges provides bonding from smaller regions of sample than bulk techniques such as nuclear magnetic resonance (NMR) and X-ray diffraction (XRD). Few chemical or spectroscopic studies have been conducted on the Be borides possibly, in part, as a result of the difficulty in analyzing for Be and B. For example, quantitative analysis of B is possible by electron microprobe analysis (EMPA) mainly with wavelength-dispersion spectrometry (WDS), but also by energy-dispersion spectrometry (EDS), whereas analysis of Be is still difficult or impossible.

The Be–B system was extensively studied during the 1960s and 1970s, and many new phases were discovered. Be borides possess low density, high hardness, and high sound speeds, and early studies were done to ascertain their potential usefulness as components of ceramic armor (1). Many questions remain about the structure of most of the phases, and there are still many uncertainties in the Be–B phase diagram. For example, the powder diffraction file (PDF) lists six Be–B phases, whereas at least 12 such phases are reported in the literature (2). Even the true equilibrium phases are not definitely known. In addition, the liquidus boundaries are uncertain for a wide range of compositions. The region with most uncertainty is between B and BeB_6, which is caused partly by the large number of polymorphs that are thought to exist in this region (see references in 2).

There is currently considerable interest in materials with the α-rhombohedral boron structure (α-rh B) since these compounds possess useful and interesting physical and chemical properties. At least two Be–B materials, BeB_{12} and $BeB_{12}C_2$, are thought to have the α-rh B structure (3, 4), but no recent studies have been conducted on these potentially useful materials; their structures and properties remain largely unknown. The two recognized Be–B–C compounds, BeB_2C_2 and $BeB_{12}C_2$ (4), have different structures and widely different physical properties.

In this paper we use parallel EELS (PEELS) with a transmission electron microscope (TEM) to determine the stoichiometry of Be borides and selected ternary Be–B–*X* materials by examining a range of commercial and laboratory-synthesized materials. Comparison of the different core-loss edges provide a qualitative understanding of the bonding within the lower part of the conduction band. In addition, we describe $Be_{0.5}B_5N$, a new material with the α-rh B structure.

2. MATERIALS AND METHODS

Commercial Be borides from Electronic Space Products International (ESPI) with reported compositions "Be_2B,"

[1] To whom correspondence is to be addressed. E-mail: lgarvie@asu.edu.

0022-4596/97 $25.00

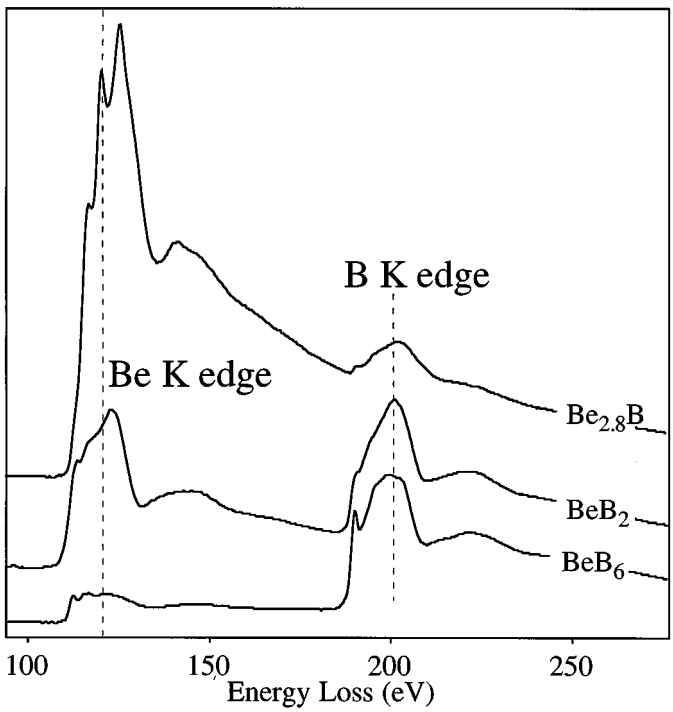

FIG. 1. Low-resolution PEELS spectra showing the Be and B K edges for selected Be borides illustrating the changes in the relative core-loss peak intensities with change in Be : B ratio.

"BeB_2", and "BeB_6" with claimed purity of 99% were studied. For our syntheses, amorphous B (99.99%), finely powdered Be (99.9%), and graphitic C (99.999%) were thoroughly mixed and packed into hexagonal BN (hBN) crucibles. The mixtures were heated in an Ar atmosphere at 1700°C for 5 h in a vertical Al_2O_3 tube furnace equipped with a Mo wire heater.

Spectra were acquired with a Gatan 666 PEELS spectrometer attached to a Philips 400ST-FEG TEM. The TEM is equipped with a thermally assisted field-emission gun (FEG) and operated at 100 keV with an emission current of 1 μA, a probe semiangle of 0.9 mrad, and a collection angle of 11 mrad. Under these conditions, the resolution of the TEM PEELS system was 0.9 eV. In cold-cathode mode (with thermal assistance turned off), a resolution of 0.7 eV was normal. The spectrometer was calibrated against the π^* peak at the B K edge of hBN, which occurs at 192.1 eV (5). Hexagonal BN was used as an internal standard so that B K edges could be calibrated to within $\pm$ 0.2 eV.

Samples were prepared by crushing the materials in methanol in a boron carbide mortar and pestle and allowing a drop of the sample in suspension to dry on a lacey C coated Cu TEM grid. To reduce C contamination in the TEM, the grid supporting the finely crushed material was placed on a 100 W light bulb for ~10 min just prior to insertion in the TEM. A thermocouple placed on the bulb gave a reading of ~170°C. Failure to place the sample on the bulb invariably resulted in the buildup of carbonaceous material during the recording of PEELS data, which was a problem since the C K edge from the contamination interfered with the C K edge from the materials under investigation.

Core-loss edges were obtained from thin areas, typically < 50 nm thick, overhanging holes in the lacy C film. Spectra for near-edge structure studies were acquired with a dispersion of 0.1 eV/channel, a 1 or 2 s acquisition time, and cold-cathode mode. At least five spectra were acquired for each edge and each spectrum was shifted by ~0.5 eV. The resulting set of data were then aligned and summed. For quantitative analysis, spectra were acquired with a dispersion of 1 eV, acquisition time of 2 s, and a thermally assisted FEG. Spectra were acquired in diffraction mode from areas of approximately 20 nm diameter. The dark current and a background of the form AR^{-r} were subtracted from beneath each core-loss edge. The high-resolution K edges were further processed by deconvoluting the effects of the asymmetry of the zero-loss peak and the point-spread function (6). The PEELS spectra were analyzed with the Gatan el/p PEELS software and the elemental ratios determined using Hartree–Slater cross sections.

3. POWDER XRD AND STOICHIOMETRY

The Be–B materials range from dark metallic, through lustrous transparent red, to adamantine, and golden yellow (Tables 1 and 2). Of the seven samples studied, we identified five binary species $Be_{2.8}B$, BeB_2, Be_4B_5, BeB_6, and crystals with compositions ranging between $BeB_{8.7}$ and $BeB_{11.6}$. In addition, we examined four ternary Be–B–*X* materials. Synthesis by products include B_4C, $Be_2BO_3(OH)$, BeO, and Be_2C. The Be borides are described with respect to decreases in the Be : B ratio, followed by the ternary Be–B–*X* materials.

3.1. $Be_{2.8}B$

The powder XRD pattern of the commercial "Be_2B" powder matches that for Be_2B in the PDF (13-315), but PEELS shows it to be $Be_{2.8(\pm 0.1)}B$. The powder XRD data of Markovsky *et al.* (7) also point to an extended field of homogeneity for this phase.

3.2. Be_4B_5

The powder XRD pattern of the commercial "Be_2B" powder contains many weak lines, also observed by Hoenig *et al.* (8). He attributed these to Be_6B, BeO, and an unknown "bright colorless phase". By TEM we observed a minor

TABLE 1
Summary of Results from the Commercial Powders

Reported phase	Visual observations	XRD and PEELS
BeB_6	Two major types of crystals: (a) golden-yellow transparent material with adamantine luster; and (b) dark gray metallic dendritic clusters. Both types are abundant.	Golden-yellow crystals range between $BeB_{8.7}$ and $BeB_{11.6}$. Metallic gray crystals have an average composition $Be_{0.6(\pm 0.1)}B_{5.9(\pm 0.7)}C$.
BeB_2	Two materials: (a) major component, gray, metallic, crystalline; and (b) minor component, red transparent and crystalline.	Major component with composition $BeB_{2.0(\pm 0.1)}$. Red component with composition $Al_{5.6(\pm 1.8)}Be_{12.7}B_{176(\pm 14.9)}$.
Be_2B	Copper-red opaque anhedral grains with metallic luster.	Major component with composition $Be_{2.8(\pm 0.1)}B$. A minor intergranular component with composition $BeB_{1.25(\pm 0.03)}$ (or Be_4B_5).

intergranular phase with composition $Be_4B_{5(\pm 0.15)}$ in the commercial "Be_2B." A similar phase, coexisting with their syntheses of Be_4B and Be_2B, was reported by Stecher and Aldinger (9). They referred to it as the η-phase and concluded that is has the formula Be_2B_3. Owing to the difficulty of determining the stoichiometry of Be–B materials from small amounts of material, it is possible that the Be_2B_3 of Stecher and Aldinger (9) with Be : B of 1 : 1.5 is the same as our Be_4B_5 with Be : B of 1 : 1.25.

3.3. BeB_2

The powder XRD pattern for the commercial "BeB_2" powder matches that for BeB_2 in the PDF (13-314); the stoichiometry by PEELS is $BeB_{2.0(\pm 0.1)}$. This composition is similar to the $BeB_{2.01(\pm 0.03)}$ result of Sands *et al.* (10). However, the material with a diffraction pattern that matches PDF 13-314 has been cited as both BeB_2 and BeB_3 in the literature (10, 11). These reports are confusing since BeB_3 and BeB_2 appear to be used interchangeably.

The source of the confusion regarding the stoichiometry results from work on BeB_3 prepared in an Al melt (11–13). These crystals actually have composition of $Al_{0.06}BeB_{3.05}$, not BeB_3. This material has also been defined as $Al_{1.42}Be_{24}B_{80.6}$ (13, and see data on PDF card 29-0008). Thus, BeB_3 and $Al_{1.42}Be_{24}B_{80.6}$ have been defined as the same material with the same lattice constants, space group, and structure. There was no evidence of Al at ca. > 0.5 at. % in our BeB_2, and our work supports earlier reports of an Al-free material with this composition.

3.4. $BeB_{6.1}$

A red crystalline powder is obtained by heating Be and B in a 1 : 6 ratio, and the resulting powder pattern matches the PDF data for BeB_6 (13-361), which is tetragonal with the αAlB_{12}-type structure (10). The PEELS spectra provided a composition of $BeB_{6.1(\pm 0.5)}$, consistent with previous analyses (8, 10).

TABLE 2
Summary of Experimental Syntheses and Results

Starting mixture	Visual observations	XRD and PEELS
12B + Be	Loosely packed powder. Under the binocular microscope two euhedral grain types are evident: transparent, golden-yellow crystals and black crystals.	Golden grains with an XRD pattern similar to B_6O and composition $Be_{0.5(\pm 0.1)}B_{4.9(\pm 0.3)}N$. The black component has an XRD pattern similar to tetragonal boron and by PEELS contains predominantly B with minor N.
6B + Be	Loosely packed powder. Brick-red transparent crystals with adamantine luster. Several minor phases are present.	The red crystalline material has an XRD pattern consistent with BeB_6 and stoichiometry of $BeB_{6.1(\pm 0.5)}$. Minor phases include B_4C, Be_2C, BeB_2, and $Be_2BO_3(OH)$.
Be + B + C	Lightly consolidated mass of black graphitic aggregates and fine-grained, tan-colored masses.	X-ray diffraction patterns and PEELS show BeB_2C_2 (black) and Be_2C (tan colored). PEELS of the BeB_2C_2 gives $BeB_{1.63(\pm 0.1)}C_{1.60(\pm 0.08)}$ (or $Be_{0.6}B_2C_2$).

3.5. $BeB_{9\text{ to }12}$

Borides with compositions between B and BeB_6 are poorly characterized because of the combination of solid solution, polymorphism, and difficulties of Be and B analysis. The structures of the B-rich phases depend on both the synthesis conditions and the initial form of the B. Several polymorphs of BeB_{12} have been reported, including a tetragonal BeB_{12} (14), trigonal BeB_{12} (with a structure akin to B_6O) (3), and possibly the BeB_{12} of Vekshina *et al.* (15).

There are two materials of roughly equal abundance in the commercial "BeB_6" powder, black and golden-yellow crystals. Powder XRD of the golden-yellow crystals produced a pattern with similarities to the BeB_{12} of Becher (14) and Vekshina (15). PEELS provides compositions ranging from $BeB_{8.7}$ to $BeB_{11.6}$.

3.6. $Be_{0.5}B_{4.9}N$

We attempted to synthesize BeB_{12}, with the α-rh B structure using the method of Kondrashev *et al.* (3) by heating Be and B with a ratio of 1 : 12 at 1700°C (Table 2). The reaction product was heterogeneous, with the top half a golden yellow and the bottom half black. Powder XRD of the golden-yellow crystals gave a pattern similar to that of B_6O, together with reflections from BeO. The *d*-spacings and intensities of the diffraction maxima from the golden-yellow material closely match the values for the BeB_{12} of Kondrashev (3), with several additional weak reflections not listed by Kondrashev, but present in the XRD pattern of B_6O (16). Refinement of the unit cell with space group $R\bar{3}m$ gives refined hexagonal cell parameters of $a_h = 5.487(5)$ Å and $c_h = 12.486(14)$ Å.

PEELS of the golden-yellow crystals provides the surprising result that this material contains major N, presumably from the hBN crucible. This material has the formula $Be_{0.5(\pm 0.1)}B_{4.9(\pm 0.3)}N$ (hereafter called $Be_{0.5}B_5N$) and represents a new member of the α-rh B-rich family along with the recently described B_6N (17, 18). Scanning electron microscopy of $Be_{0.5}B_5N$ shows crystals in the form of hexagonal dipyramids with a (0001) pinacoid (Fig. 2), similar to those of other α-rh B borides (17). The black part has powder XRD reflections from $Be_{0.5}B_5N$, BeO, and a Be boride similar to tetragonal B with the AlB_{12}-type structure (19). By PEELS, $Be_2BO_2(OH)$ was found in the black part.

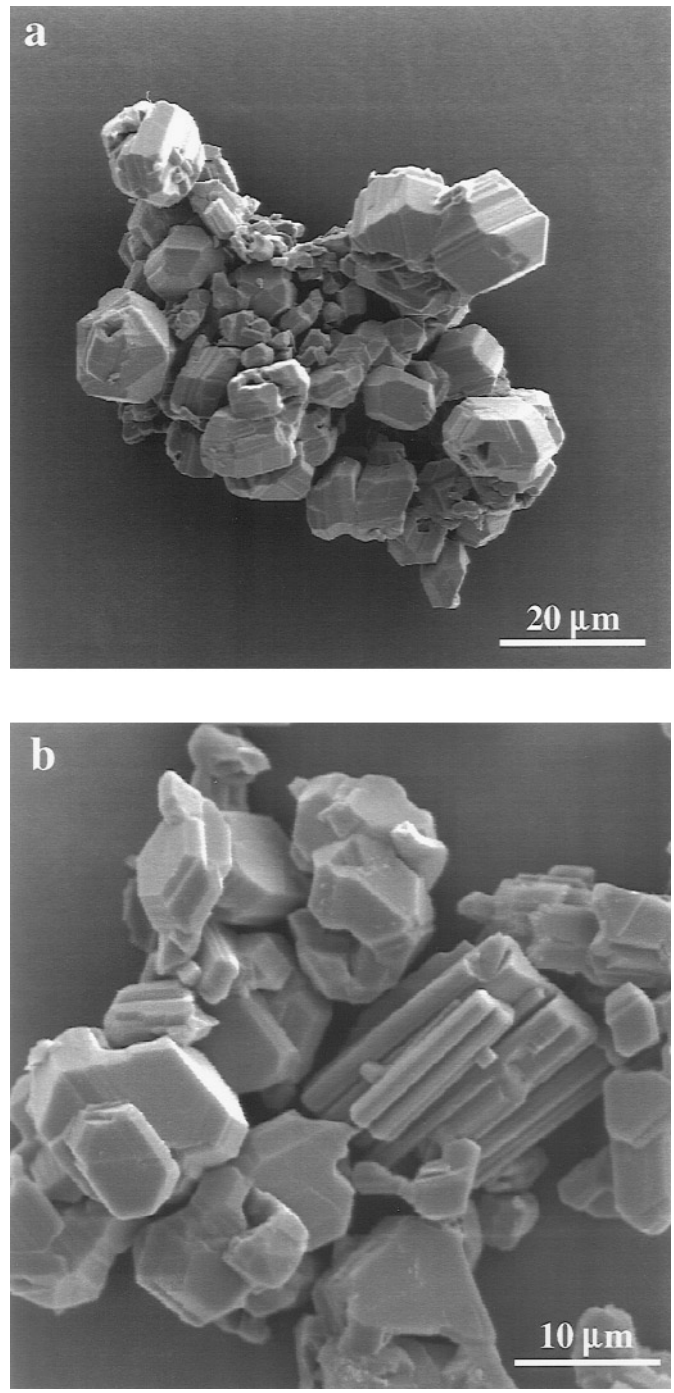

FIG. 2. Scanning electron microscope pictures of $Be_{0.5}B_5N$. (a) Sintered mass of truncated hexagonal dipyramids, and (b) associated rod-shaped aggregates of BeO.

3.7. BeB_2C_2

We synthesized BeB_2C_2 following the method of Markovskii *et al.* (4) with an excess of Be and C, the idea being that single crystals of BeB_2C_2 might grow in a matrix of Be_2C. The synthesis product is friable. The product gave XRD reflections for Be_2C and BeB_2C_2, although the lines for BeB_2C_2 are shifted from those in the PDF (24-134). Markovskii *et al.* (4) also noticed variations in the powder XRD pattern of their BeB_2C_2, which they attributed to variations in stoichiometry. The Be_2C was dissolved in boiling concentrated HCl, and the resulting powder is soft,

resembling graphite, with clusters of irregularly shaped crystals. PEELS of the BeB_2C_2 gave $BeB_{1.6(\pm 0.1)}C_{1.6(\pm 0.1)}$, close to $Be_{0.6}B_2C_2$.

3.8. $Be_{0.6}B_{5.7}C$

The black dendritic crystals in the commercial "BeB_6" powder has a powder XRD pattern similar to that of B_6O. These crystals have composition $Be_{0.6(\pm 0.1)}B_{5.9(\pm 0.7)}C$. This formula resembles the $BeB_{12}C_2$ of Markovskii *et al.* (4), which they presumed had the α-rh B-type structure with $a = 5.615$ and $c = 12.28$ Å. The diffraction pattern and the B K-edge ELNES (see below) of the black dendritic phase suggest an α-rh B-type structure similar to B_4C.

3.9. $Al_{5.6}Be_{12.7}B_{176}$

The commercial "BeB_2" contains minor amounts of a red crystalline material. PEELS of this material has composition $Al_{0.44(\pm 0.15)}BeB_{13.8(\pm 1.2)}$. The ratio of elements is similar to a known phase, $Al_{8.69}Be_{13.48}Be_{176}$ (20, and see data on PDF card 42-0928), close to our $Al_{5.6}Be_{12.7}B_{176}$.

4. ENERGY-LOSS NEAR-EDGE STRUCTURE

4.1. Introduction

The B K edges of the Be–B-bearing materials (Fig. 3) exhibit a wide range of shapes, reflecting their different bonding types. These include metallic in Be_2B (12×10^{-6} Ω cm), BeB_2C_2 (17×10^{-4} Ω cm), and BeB_2 (2×10^{-2} Ω cm); semiconducting in $Be_{0.5}B_6C$ (3.3 Ω cm); and insulating in BeB_6 and $BeB_{8\text{ to }12}$ (10 to 60×10^6 Ω cm) (21). Our discussion of the core-loss edges is restricted to the first 20 to 30 eV of ELNES above edge onset. Following the ELNES region are broader peaks—or the extended energy-loss fine structure (EXELFS)—derived from scattering of the ejected electron from the nearest neighbors (22).

The core-loss edges are a projection of the atom resolved, partial density of states (PDOS) of the conduction band. For the K edges, the PDOS represent the unoccupied *p* states for the ionized atom. For Be and B, similarities between the K ELNES correspond to mixing of local conduction-band *p* orbitals. In certain cases core-hole effects may alter features near the conduction-band onset. This effect is more likely for Be because charge transfer of valence electrons from the Be to the B reduces the screening on the Be site. In metallic materials, core-hole effects are minimized because of the screening by the itinerant outer-shell electrons.

4.2. Be and B K Edges

The B K edges for the refractory Be–B materials and accessory phase $Be_2BO_3(OH)$ are displayed in Fig. 3.

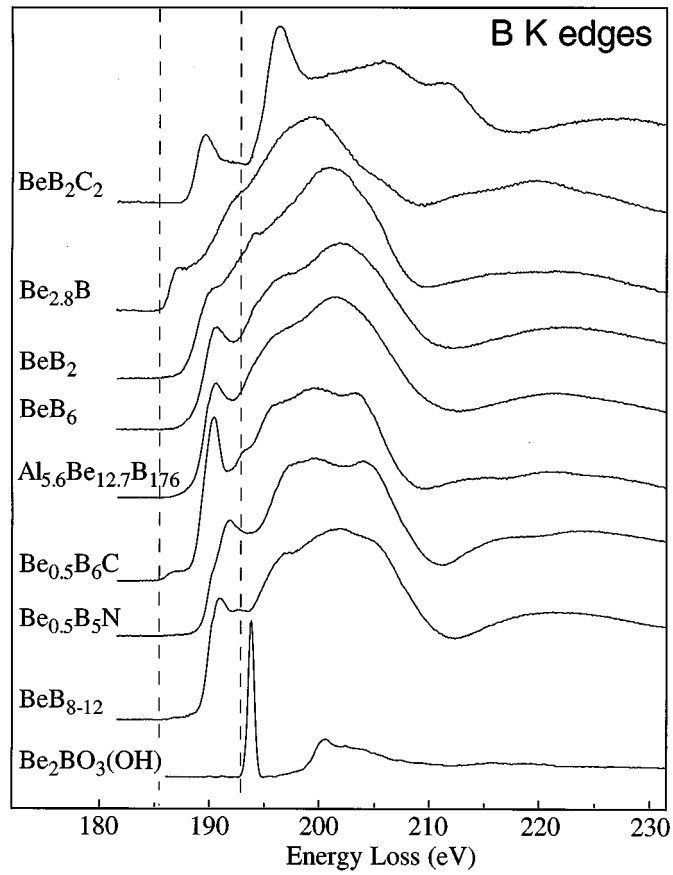

FIG. 3. B K edges of selected B-bearing materials described in the text. The dotted vertical lines mark the lowest energy onset, in Be_3B (metallic), and greatest energy onset, in $Be_2BO_3(OH)$ (insulating). The dotted lines have been set to the inflection points of the rising edges.

Except for BeB_2C_2 and $Be_2BO_3(OH)$, the B K-edge shapes exhibit similar ELNES. The rest of the Be–B-bearing materials are arranged from top to bottom with increase in energy of the edge onset. This increase also reflects the transition from metallic in Be_3B to insulating in BeB_6. All these edges have similar shapes, although Be_3B and BeB_2 do not exhibit the sharp peak at ~191 eV present at the other B K edges.

In $Be_2BO_3(OH)$, B is threefold coordinated to O, and the low-loss region of the PEELS spectrum shows a band gap of ~7.5 eV. In the BO_3^{3-} anion, the lowest unoccupied MO is the a_2'' (π^*) antibonding MO, which is derived from B 2*p* electrons. This is followed by the a_1' (σ^*) and the doubly degenerate e' (σ^*) MOs, which are predominantly B 2*s* and B 2*p* in character, respectively (23). The first sharp peak at the B K edge of $Be_2BO_3(OH)$ is attributed to transitions of B 1*s* electrons to unoccupied *p* states with π^* character. Similar π^* peaks occur at the K edges for C in the carbonate anion (24) and B in borates (5, 25), hBN (26), and BeB_2C_2, which contains B threefold coordinated to C. The π^* peak of

BeB_2C_2 has a lower energy than $Be_2BO_3(OH)$ that is related to its metallic-like conductivity and the lowering of the conduction-band onset.

The B K edge of Be_3B is broad, lacking sharp features, which we attribute to the overlap of bands as a result of its metallic conductivity. The first peak at the B K edge is at 187.4 eV, below the first feature seen in β-rh B or α-rh B (27), consistent with its metallic bonding. In $Be_{0.5}B_5N$ there is a low energy peak that occurs before the main B K-edge onset. A similar prepeak also occurs at the B K edges of B_9CO and B_6N (18). These three materials are all gray or black with a metallic luster. It is possible that the prepeak arises from transitions of the core electrons to high densities of unoccupied states within the band gap. Such trapping levels have been detected by optical measurements in β-rh B (29) and $B_{12}P_2$ (29) and found to be important for the electronic-transport properties. BeB_6, $BeB_{8\text{ to }12}$ and $Al_{5.6}Be_{12.7}B_{176}$ have similar B K edges, with an initial peak at 190.5 eV and two broad features at $\sim$197 and 201 eV.

The Be and B K edges for selected materials are compared in Fig. 4. the Be K edge has been aligned with the B K edge such that ELNES features at both edges match.

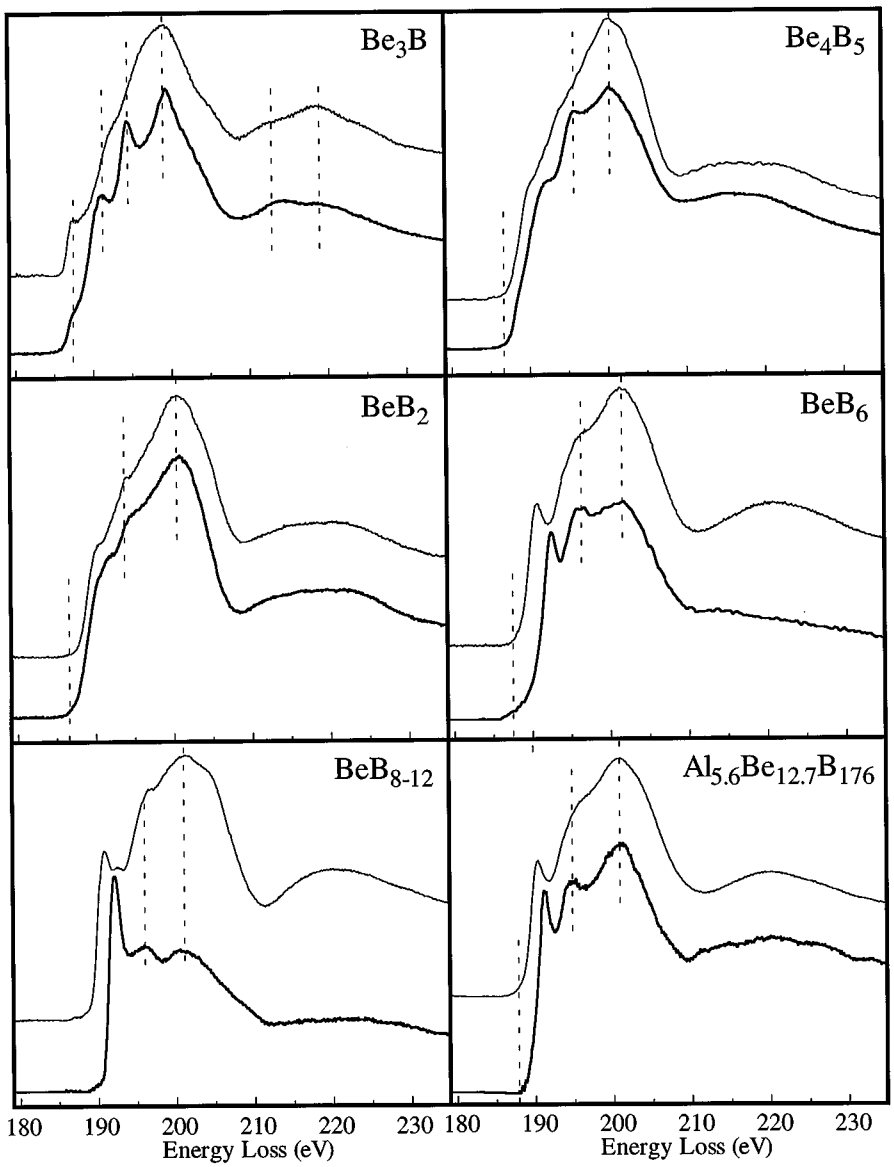

FIG. 4. Comparison between the Be (bold line) and B K edges of selected binary and ternary Be–B-bearing materials. The K edges are aligned with respect to similar energy features at the different edges. The energy scale is for the B K edge. Be energy onset is about 80 eV lower in energy. The dotted lines indicate similarities between the Be and B K edges.

The spectra can be divided into two groups; those in which the K edges match over the whole of the ELNES region, Be_3B, Be_4B_5, and BeB_2; and spectra from BeB_6, $BeB_{8\text{ to }12}$, and $Al_{5.6}Be_{12.7}B_{176}$ in which there are differences within the first 5 eV of the edge.

The B and Be K edges for Be_3B are similar over the whole of the ELNES region (Fig. 4), which suggests mixing of the Be and B states. The Be K edge in a Be_3B exhibits several sharp features whose origin is unknown and not present at the Be K edge of elemental B (unpublished data). There is close correspondence between the Be and B K edges of Be_4B_5 and BeB_2 (Fig. 4). The Be K edges are broad, indicative of mixing of conduction band states. The sharp near-edge feature of the Be K edge becomes more prominent on going from BeB_2 to Be_4B_5 and Be_3B, i.e., with an increase in the Be : B ratio and electrical conductivity.

The correspondence between the Be and B edges of BeB_6, $BeB_{8\text{ to }12}$, and $Al_{5.6}Be_{12.7}B_{176}$ (Fig. 4) is less obvious. They have been aligned with respect to near-edge features between 195 and 205 eV rather than to the sharp peaks near the edge onset. In these insulators the Be acts as a cation with charge transfer from Be to B. Because of this charge transfer, screening of the core hole is reduced, and a sharp excitonic feature forms near or below the true conduction-band edge of the cation. Such a feature is visible at the Be K edge of the three insulating materials (Fig. 4) and indicates a narrow band of unoccupied Be 2*p* character. Alignment of the K edges shows that the first 1 to 2 eV of the conduction band is dominated by B states of *p*-like symmetry with an absence of Be *p*-like states.

4.3. $Be_{0.5}B_5N$

The three K edges of $Be_{0.5}B_5N$ have been aligned as above (Fig. 5). The B K edge is similar in shape to that of B_6N and of other members of the α-rh B group (18, 27). The Be K edge is similar to that of $BeB_{8\text{ to }12}$ (Fig. 4).

The Be and B K edges align well higher in the conduction band, between E and G, but are dissimilar in the lower part of the conduction band. As described in Section 4.2, the large Be K-edge peak is a sign of core-hole effects because of charge transfer from Be. A similar Be K-edge shape was described from Be_2C (30). The similarity of the Be and B K edges higher in the conduction band can be explained by substitution of Be for B within the icosahedra. In this way there would be considerable mixing of the Be and B conduction-band states.

The N K edge aligns well with features E and F at the B and Be K edges and with D on the Be K edge. The dissimilar shape of the N K edge and the Be and B K edges higher in the conduction band can be explained if N *p* states are relatively independent of the Be and B states. This independence can be achieved if the N resides between the icosahedra. The similarity of the XRD profiles and N and O K edges of $Be_{0.5}B_5N$, B_6O and B_6N suggest a common structure. In B_6O and B_6N, the guest atoms reside in pairs between the icosahedra. Thus, the similarity of the XRD patterns and N and O K edges lends support to the siting of N_2 pairs between the icosahedra.

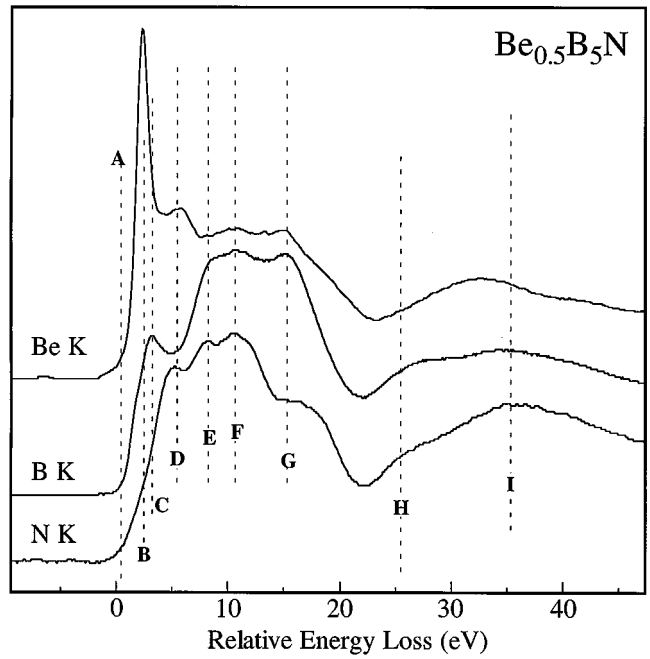

FIG. 5. Core-loss edges for $Be_{0.5}B_5N$. The features indicated by the dotted lines are discussed in the text.

4.4. BeB_2C_2

The core-loss edges of BeB_2C_2 and isostructural LiBC (31) are aligned and compared in Fig. 6. LiBC is used as an aid to align the edges of BeB_2C_2 since the edges of LiBC show similar but more pronounced features. The B K edges and the C K edges of BeB_2C_2 and LiBC show similar ELNES. In addition, there is close correspondence between the ELNES at the B and C K edges. The best alignment of the Li K edge with the C and B K edges is when its first peak is shifted 6 eV above the conduction band onset (0 eV in Fig. 6). With this alignment, its other ELNES features correspond to features at the C and B K edges. Similarly, the Be K edge can be aligned with the C and B K edges.

The agreement between the B and C K-edges shapes of BeB_2C_2 is consistent with the predominantly covalent bonding between B and C in the B–C layer. The stronger π^* peak at the B K edge relative to that at the C K edge may indicate charge transfer from B to the more electronegative C. The Be K edge parallels the increase in the intensity of the B and C K edges. The lack of a significant excitonic feature

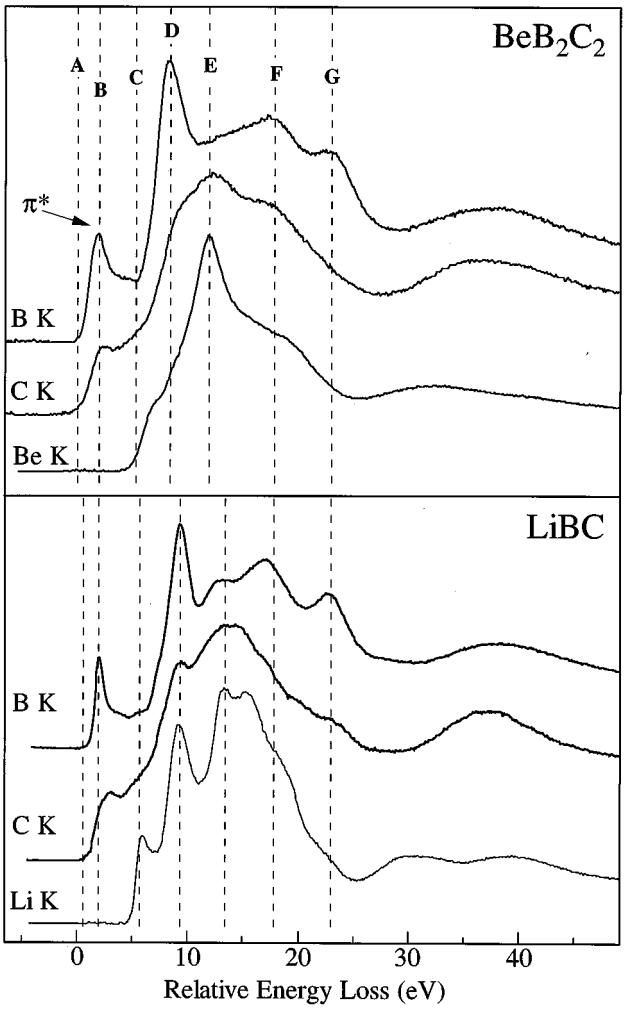

FIG. 6. Core-loss edges for BeB_2C_2 and LiBC. The features indicated by the dotted lines are discussed in the text.

at the Be K edge and the good agreement between the three K edges indicate predominantly covalent bonding between Be and the B–C sheet. The near-edge structure at the edge onset is dominated by B and C states of *p*-like symmetry without contribution from Be *p* states.

5. CONCLUSIONS

PEELS with a TEM is well suited for characterizing Be–B-bearing materials. The Be and B K edges are well separated in energy, allowing easy determination of the elemental ratios. In addition, the ELNES of the core-loss edges provides qualitative information about the bonding and local band structure.

It is clear from this study that materials that contain Be and B have complex structures and stoichiometries. Many issues remain unsolved because of the difficulties of light-element analysis using conventional analysis techniques. Our PEELS analyses of "Be_2B" and "Be_2B_3" provided stoichiometries of $Be_{2.8}B$ and Be_4B_5, respectively. The case of BeB_2 versus BeB_3 has now largely been solved although the existence of BeB_3 is now in doubt. We confirmed earlier reports of Be borides with compositions of BeB_2 and BeB_6.

We confirmed an earlier report of a Be–B–C phase with the α-rh B structure and also synthesized and characterized a new ternary Be–B–N phase, $Be_{0.5}B_5N$, with the α-rh B structure. By comparing the core-loss edges from $Be_{0.5}B_5N$, we conclude that the N predominantly forms N_2 pairs between the icosahedra and Be substitutes for B within the icosahedra.

ACKNOWLEDGMENTS

We thank David Wright of the Materials Facility, Center for Solid State Science at Arizona State University for help with the Be boride syntheses and Dr. Wörle for the LiBC. This work was supported by grants from the National Science Foundation NSF EAR-9418206 (to PRB and LAJG) and DMR 903-6253 (to PR). The PEELS used for this research was performed at the Center for High Resolution Electron Microscopy at Arizona State University, established with support from the National Science Foundation (DMR-89-13384).

REFERENCES

1. M. L. Wilkins, "Boron and Refractory Borides" (V. I. Matkovich, Ed.), p. 631. Springer-Verlag, New York, 1971.
2. H. Okamoto and L. E. Tanner, "Phase Diagrams of Binary Beryllium Alloys," Vol. 21. ASM International, Ohio, 1987.
3. Y. D. Kondrashev, G. S. Markevich, and L. Y. Markovskii, *Russ. J. Inorg. Chem.* **11,** 780 (1966).
4. L. Y. Markovsky, N. V. Vekshina, Y. D. Kondrashev, and I. M. Stroganova, *J. Appl. Chem. USSR* **39,** 10 (1966).
5. L. A. J. Garvie, A. J. Craven, and R. Brydson, *Am. Miner.* **80,** 1132 (1995).
6. R. F. Egerton, "Electron Energy-Loss Spectroscopy in the Electron Microscope," Plenum, New York, 1986.
7. L. Y. Markovsky, Y. D. Kondrashev, and G. V. Kaputovskaya, *J. Gen. Chem. USSR* **25,** 1007 (1955).
8. C. L. Hoenig, C. F. Cline, and D. E. Sands, *J. Am. Ceram. Soc.* **44,** 385 (1961).
9. J. Stecher and F. Aldinger, *Z. Metallkde.* **64,** 684 (1973).
10. D. E. Sands, C. F. Cline, A. Zalkin, and C. L. Hoenig, *Acta Crystallogr.* **14,** 309 (1961).
11. R. Mattes, K. F. Tebbe, H. Neidhard, and H. Rethfeld, *J. Less-Common Met.* **47,** 29 (1976).
12. R. Mattes, H. Neidhard, H. Rethfeld, and K. F. Tebbe, *Inorg. Nucl. Chem. Lett.* **9,** 1021 (1973).
13. R. Mattes, H. K. F. Tebbe, Neidhard, and H. Rethfeld, *Z. Anorg. Allg. Chem.* **413,** 1 (1975).
14. H. J. Becher, *Z. Anorg. Chem.* **321,** 217 (1966).
15. N. V. Vekshina, L. Y. Markovskii, Y. D. Kondrashev, and I. M. Stroganova, *J. Appl. Chem. USSR* **42**, 1168 (1969)
16. H. Hubert, L. A. J. Garvie, B. Devouard, P. R. Buseck, W. T. Petuskey, and P. F. McMillan, *Chemistry of Materials*, in press.
17. H. Hubert, L. A. J. Garvie, P. R. Buseck, W. T. Petuskey, and P. F. McMillan, *J. Solid State Chem.* **133,** 356 (1997).

18. L. A. J. Garvie, H. Hubert, P. R. Buseck, W. T. Petuskey, and P. F. McMillan, *J. Solid State Chem.* **133,** 365 (1997).
19. C. P. Talley, S. LaPlaca, and B. Post, *Acta Crystallogr.* **13,** 271 (1960).
20. I. Higashi, *J. Solid State Chem.* **32,** 201 (1980).
21. V. S. Neshpor and G. V. Samsonov, *Inorg. Mater.* **7,** 45 (1971).
22. P. Rez, "Transmission Electron Energy Loss Spectrometry in Materials Science" (M. M. Disko, C. C. Ahn, and B. Fultz, Eds.), p. 107. The Minerals, Metals and Materials Society, Warrendale, Illinois, 1992.
23. D. J. Vaughan and J. A. Tossell, *Am. Miner.* **58,** 765 (1973).
24. L. A. J. Garvie, A. J. Craven, and R. Brydson, *Am. Miner.* **79,** 411 (1994).
25. H. Sauer, R. Brydson, P. N. Rowley, W. Engel, and J. M. Thomas, *Ultramicroscopy* **49,** 198 (1993).
26. J. Moscovici, G. Loupias, PH. Parent, and G. Tourillon, *J. Phys. Chem. Solids* **57,** 1159 (1996).
27. L. A. J. Garvie and P. R. Buseck, submitted for publication.
28. H. Werheit, *Jpn. J. Appl. Phys.* **10,** 66 (1993).
29. H. Werheit, U. Kuhlmann, K. Shirai, and Y. Kumashiro, *J. Alloys Comp.* **233,** 121 (1996).
30. M. M. Disko, J. C. H. Spence, O. F. Sankey, and D. Saldin, *Phys Rev. B* **33,** 5642 (1986).
31. M. Wörle, R. Nesper, G. Mair, M. Schwarz, and H. G. v. Schnering, *Z. Anorg. Allg. Chem.* **621,** 1153 (1995).